



Tensile behaviour of thermally-stable nanocrystalline bainitic-steels

G.M.A.M.El Fallah*, H.K.D.H. Bhadeshia

Materials Science and Metallurgy, University of Cambridge, 27 Charles Babbage Road, Cambridge CB3 0FS, UK



ARTICLE INFO

Keywords:

Nanostructured bainite
Thermodynamic stability
Tensile tests
Austenite reversion
TRIP
Work hardening

ABSTRACT

The deformation behaviour of two nanostructured bainitic steels designed specifically to ensure the thermal stability of the retained austenite present alongside the bainitic ferrite, has been studied as a function of test temperature. One of the alloys is especially rich in silicon whereas the other in nickel. Surprisingly, the alloys are found to have greater ultimate tensile strengths and ductility when tested at 200 °C, compared with corresponding tests at ambient temperature. This is demonstrated to be a consequence of the more gradual deformation-induced transformation of the retained austenite at 200 °C. In contrast, there is a dramatic reduction in both strength and uniform ductility during testing at 450 °C. Some carbides precipitate during testing of the high-silicon alloy, thus making the austenite less stable to both thermally and mechanically. The high-nickel alloy suffers from the same fate but for different reasons, that the austenite actually grows at the 450 °C test temperature, leading to a reduction in its thermodynamic stability.

The experimental data on the stability of the retained austenite both at the test temperature and during cooling from that temperature have been modelled.

1. Introduction

In steels, there is a temperature regime where none of the atoms can diffuse during the course of transformation from undercooled austenite. The change in crystal structure on transformation is, therefore, achieved by a homogeneous deformation of the lattice [1]. The transformation of austenite into bainite falls in this regime of limited atomic mobility so the plates of bainite grow without diffusion, but carbon can redistribute or precipitate shortly after transformation. A major consequence of this displacive mechanism is that the transformation product is in the form of thin plates, a natural mechanism of grain refinement that does not require any thermomechanical processing. This makes the bainitic steels strong and tough, provided that cementite precipitation is avoided. Silicon additions play a critical role here in retarding this precipitation [2–4], so that any carbon partitioned from the supersaturated bainitic ferrite ends up in the residual austenite that is then retained to further enhance the toughness. Solute such as nickel assist in the alloy design by affecting the hardenability and toughness of the steel [5,6]. Furthermore, the plates of bainitic ferrite become even more slender as the transformation temperature is reduced [7,8]; this is the basis of the design of nanostructured bainitic steels of the type described in this paper [9,10].

Significant headway has been made in uncovering the mechanism by which nanostructured bainite forms, and how its elementary

mechanical properties such as strength and ductility may be controlled [9,11,12]. There are now some fifty alloy-variants of the basic nanostructure under investigation in many parts of the world [Table 14.6, 11]. The two-phase mixture of slender plates of bainitic ferrite embedded in retained austenite is characterised by an extraordinarily large density of α_b/γ interfaces ($\approx 10^8 \text{ m}^{-2}$). To put this into context, the density of interfaces is greater than achieved during severe plastic deformation [Table 1, 10]. And yet, the material can, and has, been made in huge quantities with objects large in all three dimensions. The austenite instils a work hardening mechanism during deformation, thus avoiding the early plastic instability that is common in ductile nanostructured materials [13]. The production of nanostructured bainite that is generated by heat treatment alone, does not require deformation or rapid cooling.

With one exception, the reported work is on nanostructured bainite that is not resistant to prolonged tempering at temperatures in excess of about 400 °C; in particular, the retained austenite is prone to decompose into a mixture of cementite and ferrite [14–16]. However, two bulk nanocrystalline bainitic steels have recently been developed in which the austenite is much more resistant to thermal decomposition [17,18]. These alloys form the basis of a specific structural characterisation reported here, where we examine in detail the mechanical and thermal stability of the austenite at a variety of test temperatures.

* Corresponding author.

E-mail address: gmae2@cam.ac.uk (G.M.A.M.E. Fallah).

<https://doi.org/10.1016/j.msea.2018.12.124>

Received 11 December 2018; Received in revised form 29 December 2018; Accepted 31 December 2018

Available online 07 January 2019

0921-5093/ Crown Copyright © 2019 Published by Elsevier B.V. This is an open access article under the CC BY license (<http://creativecommons.org/licenses/by/4.0/>).

Table 1
Chemical compositions, wt%, austenitisation temperature (T_y) and time (t_y).

Alloy	C	Si	Ni	Al	Mo	Mn	Co	Cr	T_y / °C	t_y / h
A	0.72	3.87	3.40	1.39	0.21	0.02	< 0.01	< 0.01	260	24
B	0.45	0.03	13.20	2.63	0.30	0.15	3.99	<.005	250	120

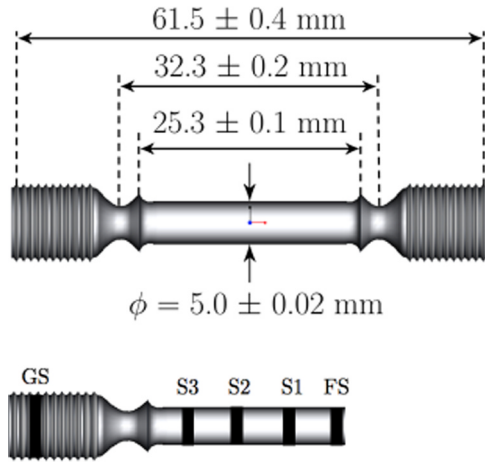


Fig. 1. Sample geometry for tensile testing. The lower diagram shows the shaded regions from which samples were extracted for X-ray diffraction analysis. The terminology is explained later in the text.

2. Materials and experimental procedures

The chemical compositions of the alloys studied are listed in [Table 1](#). Both are designed to generate a mixed nanostructure of bainitic ferrite plates embedded in a matrix of carbon-enriched austenite. They have enough carbon to ensure the low transformation temperatures to achieve the nanostructure, but Alloy A has more than the usual amount of silicon added to suppress cementite precipitation. From elementary hardenability considerations, the reduced manganese concentration avoids the need for long transformation times. Alloy B is rich in nickel and contains cobalt and aluminium additions, which enhance the thermal stability of the austenite. The alloys and the heat treatments described later were designed in another study [19].

Alloy A was produced as a 54 kg steel cast and forged to a final cross-section 57 mm × 83 mm with a 7:1 reduction ratio. Alloy B was

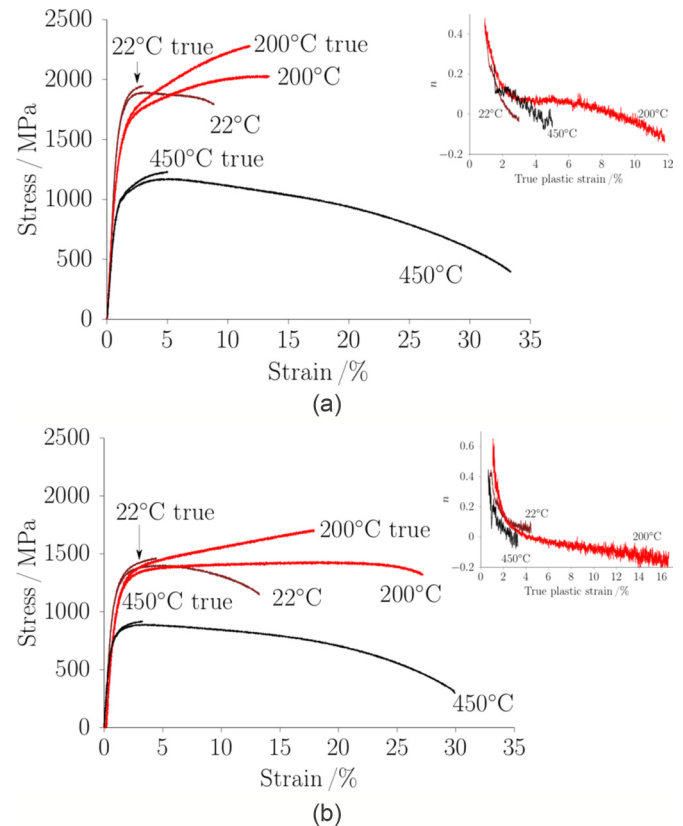


Fig. 3. True and engineering stress-strain curves as a function of test temperature, together with derived strain hardening characteristics. (a) Alloy A. (b) Alloy B.

produced by casting and hot-rolling into plate 120 mm × 20 mm × 600 mm or bars ≈ 25 mm diameter, 600 mm length.

Each sample was transformed as a blank ≈ 12 mm diameter, 70 mm length with mechanical test specimens machined subsequently from the centre of each blank to avoid any decarburised regions. Heat treatment consisted of austenitisation at 1000 °C for 30 min in a box furnace, followed by isothermal transformation at 250 °C in a fluidised bed. In the case of Alloy A, the transformation temperature was increased to 260 °C after observing a small amount of martensitic transformation on cooling to 250 °C, [Table 1](#).

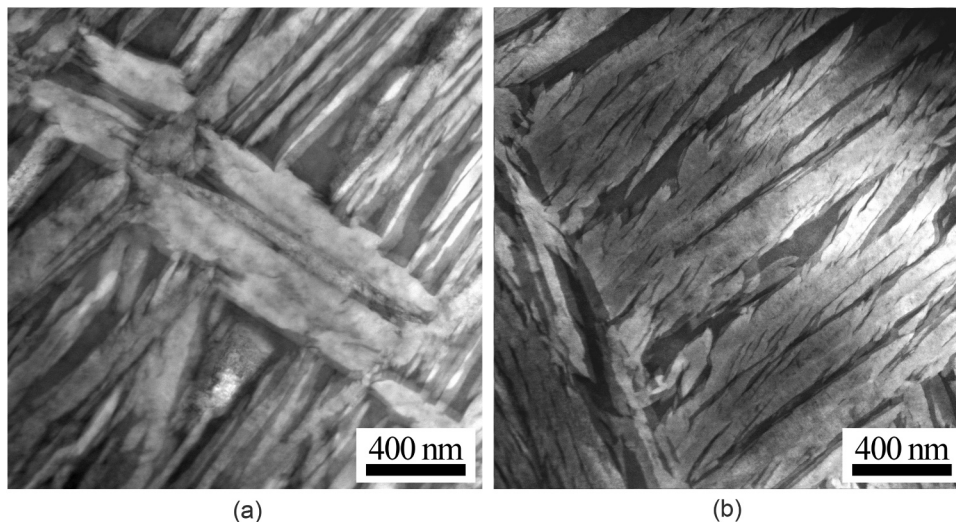
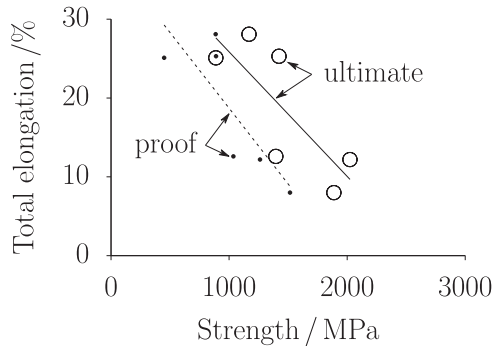


Fig. 2. STEM bright field images for the as-transformed condition, showing mixtures of bainitic ferrite and retained austenite. (a) Alloy A. (b) Alloy B.

Table 2

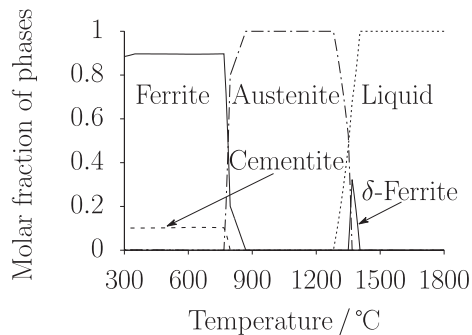
Mechanical properties for Alloy A and Alloy B. σ_{PS} and σ_{UTS} are the proof and ultimate tensile strengths respectively, ϵ_U & ϵ_T are the uniform and total elongations respectively, and ϵ_A is the reduction of area.

Alloy	Test temperature °C	0.2% σ_{PS} MPa	σ_{UTS} MPa	ϵ_U %	ϵ_T %	ϵ_A %
A	ambient	1516	1888	3.1	8.0	25.3
	200	1262	2024	12.7	12.2	16.5
	450	886	1169	4.1	28.1	79.9
B	ambient	1036	1396	4.8	12.6	48.6
	200	889	1423	18.7	25.3	40.4
	450	695	888	3.3	25.1	84.4

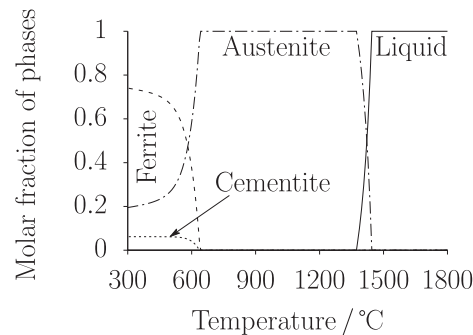
**Fig. 4.** Ductility of all six tensile tests plotted together as a function of strength.**Table 3**

Diffraction data for both alloys tested at the temperature at indicated. † tensile test at 200 °C was stopped when the plastic strain reaches the failure elongation of the ambient temperature sample.

Alloy	Test temperature / °C	Section	V_γ	$a_\gamma / \text{Å}$	$C_\gamma / \text{wt\%}$
A	ambient	FS	0.03 ± 0.01	–	–
		GS	0.28 ± 0.01	3.6332 ± 0.0052	1.44 ± 0.03
	200 °C	FS	0	–	–
		GS	0.26 ± 0.02	3.6360 ± 0.0031	1.52 ± 0.01
	450 °C	FS	0	–	–
		GS	0.22 ± 0.01	3.6246 ± 0.0042	1.18 ± 0.04
B	ambient	FS	0.04 ± 0.02	–	–
		GS	0.27 ± 0.02	3.6457 ± 0.0016	1.65 ± 0.02
	200 °C	FS	0.01 ± 0.02	–	–
		GS	0.25 ± 0.02	3.6360 ± 0.0018	1.36 ± 0.02
	200 °C †	FS	0.13 ± 0.01	3.6309 ± 0.0050	1.20 ± 0.04
		GS	0.02	–	–
450 °C	FS	0.02	–	–	
	GS	0.28 ± 0.01	3.6299 ± 0.015	1.18 ± 0.03	



(a)



(b)

Fig. 5. Phase fractions were calculated using the commercial software *ThermoCalc* and the thermodynamic database TCFE8. (a) Alloy A is predicted to be completely austenitic between 870 °C and 1270 °C. (b) Alloy B is predicted to be completely austenitic between 650 °C and 1390 °C.

Tensile tests on samples with the dimensions illustrated in Fig. 1, were carried out at ambient temperature, 200 °C and 450 °C. A constant crosshead speed of 0.002 mm min⁻¹ was maintained with samples instrumented with an extensometer that allowed the load-displacement data to be tracked. The incremental work hardening exponent was calculated as $n = d(\ln \sigma)/d(\ln \epsilon_p)$, where σ is the stress and ϵ_p the plastic strain. Vicker's hardness determinations used a 10 kg load, taking the average of six indents in each case.

Samples mounted in conductive bakelite were ground using silicon carbide emery papers (1200-grade to 2500-grade), followed by polishing with 6 μm, 1 μm finishes using diamond paste, finishing with 0.25 μm colloidal silica for scanning electron microscopy on a FEI Nova NanoSEM operating at 15 kV. Etching was with a 2% nitric acid, 98% methanol mixture. Unmounted sections were similarly prepared for X-ray analysis.

For transmission electron microscopy on a FEI Tecnai Osiris transmission electron microscope operated at 200 keV, samples were cut as 3 mm diameter discs from the broken tensile specimens, then thinned down to 0.05 mm, with final electropolishing into a thin foil using 5% perchloric acid, 25% glycerol and 70% ethanol at 8.5 °C and 25 V.

X-ray diffraction analysis (Bruker D8 DAVINCI, Cu K α radiation) was used to determine the fraction of retained austenite (V_γ) and its carbon content (C_γ). The machine was operated with a step size 0.050° with dwell time of 5 s, 2.5° primary slit, a divergence slit 8 mm wide and 18 mm antiscatter slit at 40 kV and 40 mA and a rotational speed was 30° min⁻¹. The results were subjected to Rietveld refinement [20]. The weighted profile R-factor (R_{wp}) and goodness-of-fit were used to assess the quality of fitting, which also checked graphically [21].

The Dyson and Holmes [22] relationship between the austenite composition and its lattice parameter was used to estimate its carbon content. Dilatometric samples 3 mm and length 10 mm were heated up to 500 °C, 4500 °C, 300 °C and 200 °C at a rate of 5 °C s⁻¹, held at these temperatures for 10 h, then cooled to room temperature at the same rate. These experiments were conducted on a Bähr DIL 805 A dilatometer.

3. Results and discussion

3.1. As-transformed microstructures

Representative scanning transmission electron micrographs of the two alloys following the heat treatments listed in Table 1 are presented in Fig. 2, showing the expected two-phase mixtures of bainitic ferrite and retained austenite.

3.2. Mechanical behaviour

The raw tensile test data are presented in Fig. 3, with derived

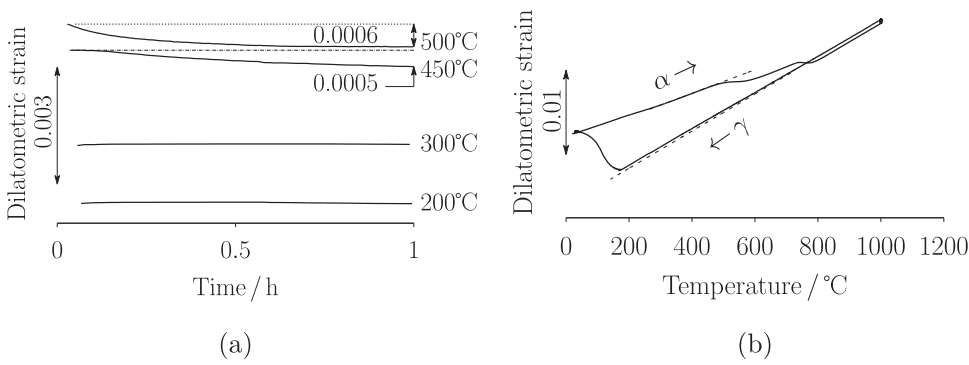


Fig. 6. Alloy B. (a) Isothermal experiments to show austenite formation as indicated by a contraction as a function of time. (b) A typical heating and cooling curve showing the linear transformation strain, i.e. the vertical distance at 450 °C between the dashed lines, as a function of temperature. From Figs. 6a and b the amount of the austenite is expected to form during the tensile test at 450 °C is $\approx 10\%$.

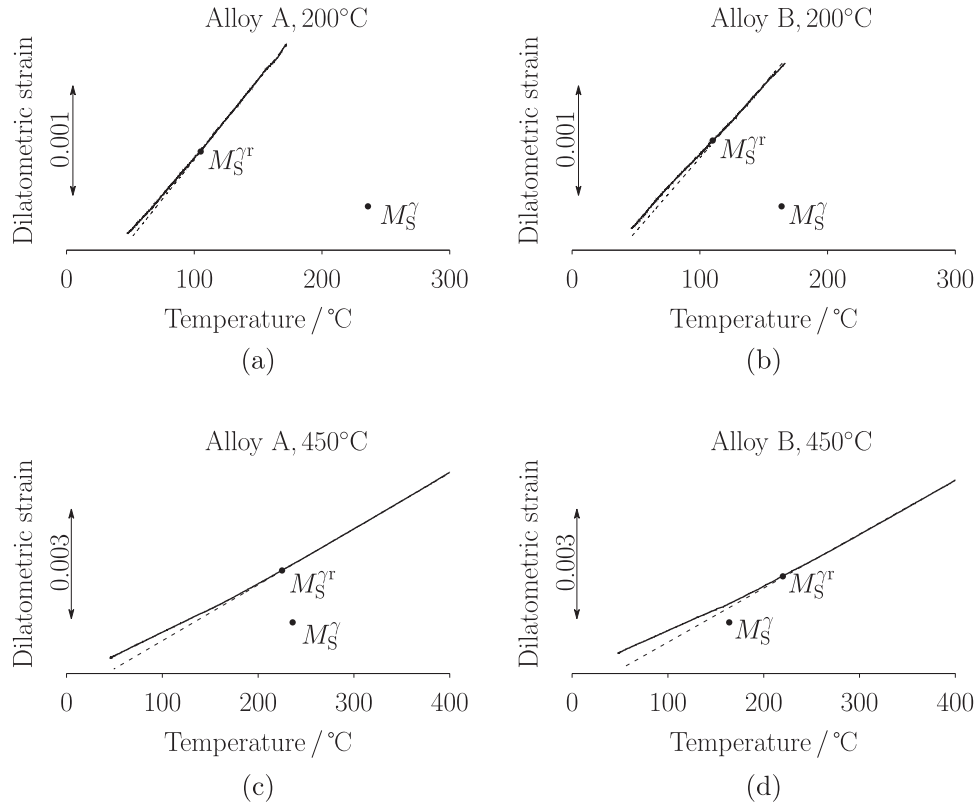


Fig. 7. The dilatation curves for the bainitic samples with deformation of 5% at the temperature indicated. $M_S^{\gamma^r}$ is martensite start temperature for the retained austenite structure and M_S^{γ} is martensite start temperature for the case where the alloy is fully austenitic.

Table 4

Measured Vickers hardness of tensile test samples, using a 10 kg load. “Change” refers to the difference in hardness between the fracture and grip regions.

Alloy	Tensile test temperature	Fracture surface	Grip section	Change
A	ambient	626 ± 18	577 ± 10	49 ± 28
	200 °C	656 ± 16	581 ± 13	75 ± 29
	450 °C	597 ± 9	590 ± 16	7 ± 25
B	ambient	543 ± 9	460 ± 11	83 ± 20
	200 °C	602 ± 20	435 ± 13	167 ± 33
	450 °C	610 ± 20	496 ± 12	113 ± 32

parameters listed in Table 2. Consistent with expectations, the higher carbon Alloy A is stronger and its performance compares well with other nanocrystalline steels rich in silicon [23].

Linear regression analysis indicates that about 60–66% of the variation in ductility can be understood in terms of the strength (Fig. 4), because stronger steels in general strain harden more rapidly, causing

the ultimate tensile strength to be reached at a smaller uniform strain. To understand the residue of the elongation, the mechanical and thermal stability of the retained austenite was examined in detail.

4. Retained austenite

The ductility of TRIP-assisted steels is, often justifiably, correlated to its retained austenite content. In essence, the deformation-induced transformation of austenite into hard martensite leads to work hardening that delays the onset of plastic instability. However, the data presented in Table 3 do not lend themselves to a simple interpretation.

For example, with δ -TRIP steel, tensile tests conducted at ambient temperature exhibited greater ductility than when tested at 100 °C [24]. The thermodynamic stability of austenite increases at higher temperatures, so when tested at 100 °C, the austenite did not transform, leading to a reduced work-hardening rate and hence a smaller uniform ductility. Contrary to those observations, the ductility in the present case actually increases when the tensile tests are conducted at

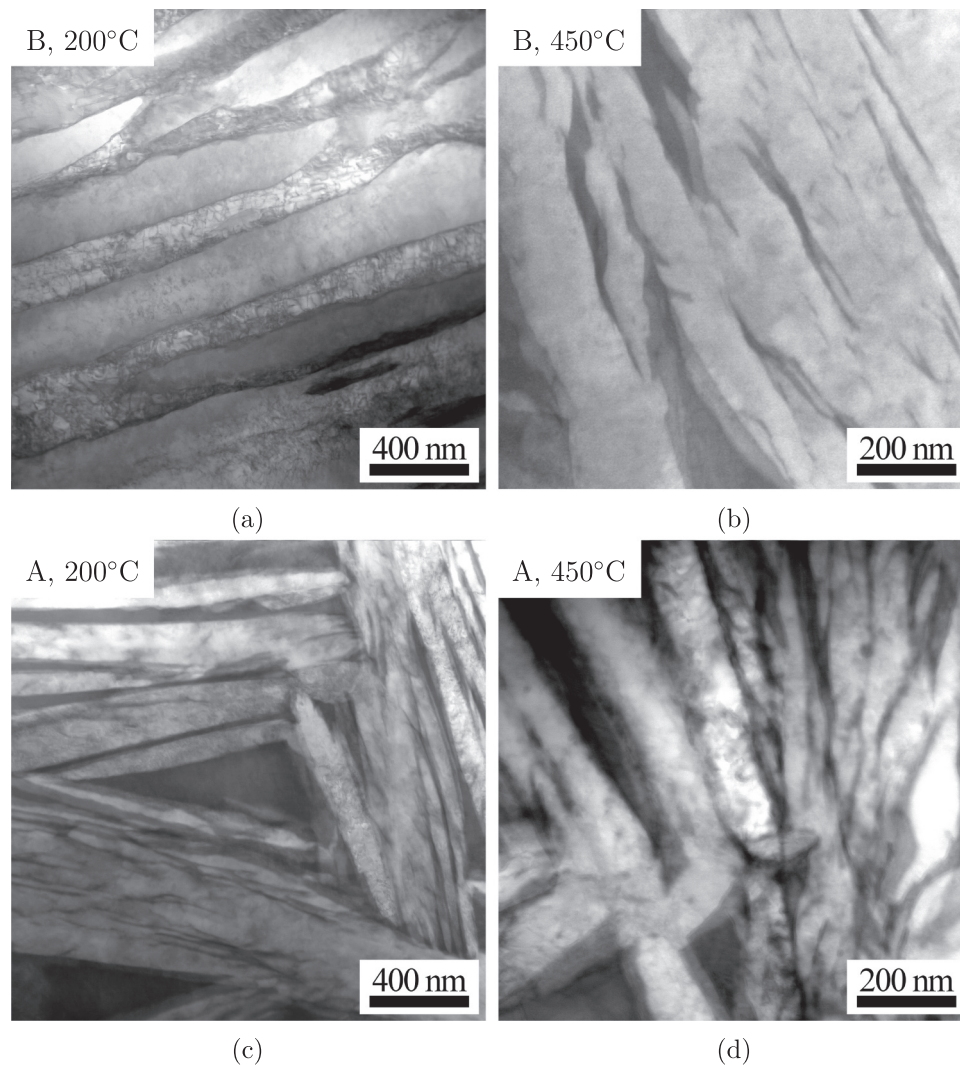


Fig. 8. Transmission electron micrographs. (a) Alloy B, following tensile testing at 200 °C. (b) Alloy B, after testing at 450 °C. (c) Alloy A, following tensile testing at 200 °C. (d) Alloy A, after testing at 450 °C.

200 °C even though the ultimate strength is greater than those tested at ambient temperature.

The greater uniform elongation in the 200 °C sample could be due to the more gradual transformation of retained austenite. This was confirmed by interrupting a test at 200 °C when the plastic strain reached the failure elongation of the ambient temperature sample, at which point almost half of the austenite remained untransformed (Table 3), whereas little austenite remained in the ambient temperature sample.

Before commenting on the elevated temperature tests, it is important to appreciate that the austenite contents listed in Table 3 were measured at ambient temperature rather than at the test temperature. As will become obvious shortly, there are strong indications that some of the austenite, *during cooling* from the deformation temperature, transforms into martensite. Furthermore, the 450 °C data indicate that there is a significant *decrease* in the carbon concentration of the retained austenite in the unstressed gauge section of the tensile specimen. This indicates structural changes other than martensitic transformation. Assuming that the thermal activation available at 450 °C is adequate, the calculated equilibrium phase diagrams (Fig. 5) indicate that it is possible for carbides to precipitate during the course of the test in the case of Alloy A, and that additional austenite may form in Alloy B. Both of these phenomena could lead to a reduction in the carbon concentration of the austenite. Experiments were conducted to investigate this further.

5. Austenite reversion in Alloy B

The experiments here were done on the bainitic samples generated using the heat treatments described in Table 1. The aim was to study whether additional austenite would form at 450 °C; only the results for Alloy B are reported because austenite growth was not detected in the case of Alloy A, consistent with the calculated equilibrium phase diagrams.

Fig. 6a showing that a significant amount of austenite forms during treatment at 450 and 500 °C as revealed by the isothermal contraction strains. An approximate measure of how much additional austenite forms is given by comparing the total transformation strain when all of the microstructure converts into austenite at any given temperature (Fig. 6b), with the observed contraction strain in Fig. 6a.

The importance of these observations is that some austenite is expected to form during the 450 °C tensile tests for Alloy B, consistent with the observed reduction in the carbon concentration (Table 3) due to dilution. The dilution should make the austenite less stable to martensitic transformation. To prove this, experiments were conducted on the bainitic samples using a deformation dilatometer. The samples were heated to the temperature at which tensile tests had been conducted, deformed plastically by 5% in compression, and allowed to cool to ambient temperature at a rate of 5 °C s⁻¹. The strain monitored could then be used to assess whether the deformed austenite transformed

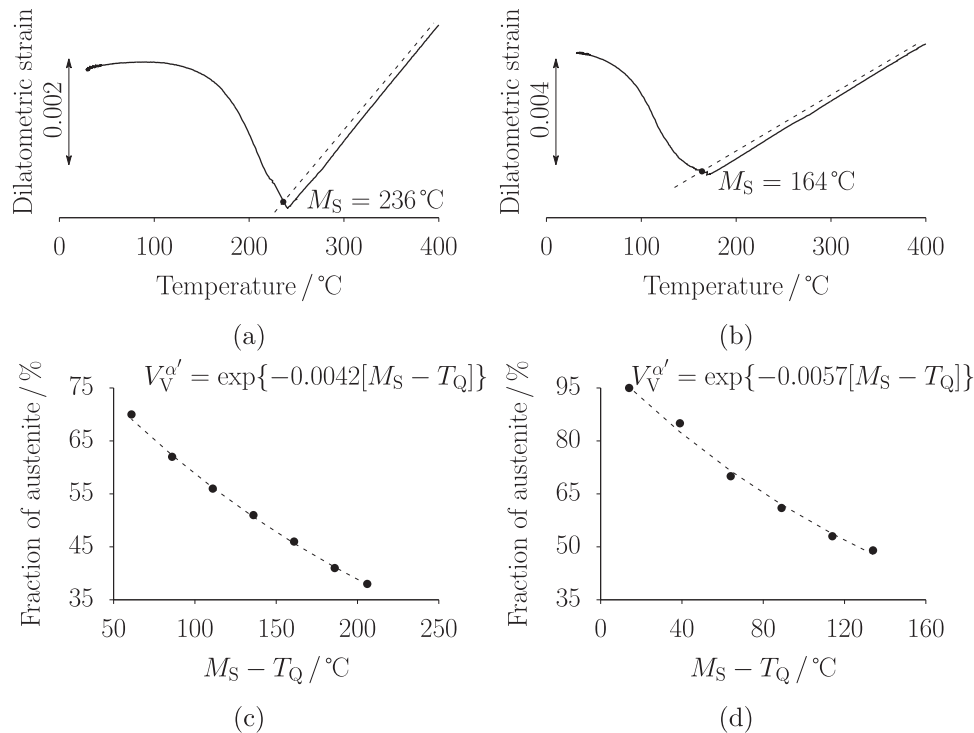


Fig. 9. Dilatometric experiments to measure the martensite-start temperatures of (a) Alloy A, (b) Alloy B. The dashed lines represent the offset at which the start temperature is defined, as described in [27]. Derivation of the Koistinen-Marburger coefficient for (c) Alloy A, (d) Alloy B.

Table 5

Calculated and measured fractions of martensite following deformation at the temperatures indicated. Note that ϵ refers to the *local* plastic strain at which the retained austenite content was determined in order to deduce $V_V^{\alpha'}$.

	Alloy A				Alloy B			
	ϵ	$M_S^g/^\circ\text{C}$	$V_V^{\alpha'}$ calculated	$V_V^{\alpha'}$ measured	ϵ	$M_S^g/^\circ\text{C}$	$V_V^{\alpha'}$ calculated	$V_V^{\alpha'}$ measured
25 °C	0.000	0	0.000	0.000 ± 0.01	0.000	0	0.000	0.000 ± 0.01
	0.031	73	0.051	0.040 ± 0.01	0.047	188	0.140	0.064 ± 0.02
	0.067	81	0.059	0.045 ± 0.01	0.074	197	0.146	0.067 ± 0.02
	0.150	118	0.092	0.095 ± 0.01	0.161	205	0.150	0.096 ± 0.02
	0.253	274	0.184	0.184 ± 0.04	0.486	323	0.191	0.232 ± 0.03
200 °C	0.000	0	0.000	0.000 ± 0.01	0.000	0	0.000	0.000 ± 0.01
	0.074	237	0.167	0.179 ± 0.01	0.233	212	0.153	0.136 ± 0.02
	0.112	274	0.181	0.195 ± 0.01	0.257	231	0.160	0.155 ± 0.02
	0.131	301	0.194	0.200 ± 0.01	0.314	307	0.187	0.214 ± 0.02
	0.165	329	0.204	0.257 ± 0.03	0.404	326	0.192	0.238 ± 0.03
450 °C	0.000	0	0.000	0.000 ± 0.01	0.000	0	0.000	0.000 ± 0.01
	0.186	227	0.162	0.190 ± 0.01	0.086	177	0.135	0.085 ± 0.02
	0.318	261	0.178	0.205 ± 0.01	0.179	207	0.151	0.123 ± 0.02
	0.609	302	0.195	0.210 ± 0.01	0.450	282	0.179	0.161 ± 0.02
	0.799	352	0.212	0.215 ± 0.03	0.844	590	0.224	0.259 ± 0.04

during cooling to ambient temperature. Fig. 7 shows, as predicted, that a significant amount of martensitic transformation occurs during the cooling of the samples deformed at 450 °C. This is not the case for the samples deformed at 200 °C. Furthermore, the martensite-start temperatures M_S^{gT} of the *retained austenite* in the 450 °C deformed samples are close to or greater than when the alloy is fully austenitic (M_S^g), Fig. 7.

Hardness measurements presented in Table 4 confirm the dilatometric data. A comparison of the grip and fracture regions, shows that Alloy B samples tested at 450 °C hardened significantly when compared with the same test for Alloy A. It is the martensite that forms during cooling from the tensile test temperature that is responsible for this. The main conclusion is that during testing at 450 °C, the austenite in Alloy B will not undergo deformation-induced transformation, but rather, will

increase in volume fraction, the resulting dilution leading to martensitic transformation during cooling. This explains the minimal work hardening in the 450 °C tensile curve illustrated in Fig. 3b.

6. Cementite precipitation

Transmission electron micrographs are presented in Fig. 8 of samples extracted from the hot tensile tests. They show that there was no detectable carbide formation when Alloy B was tested at either 200 or 450 °C. Alloy A on the other hand, revealed precipitation in the sample tested at 450 °C, explaining the reduction in the carbon concentration of the austenite following testing (Table 3). Diffraction patterns and dark-field images are presented as supplemental data (Figs. 11 and 12).

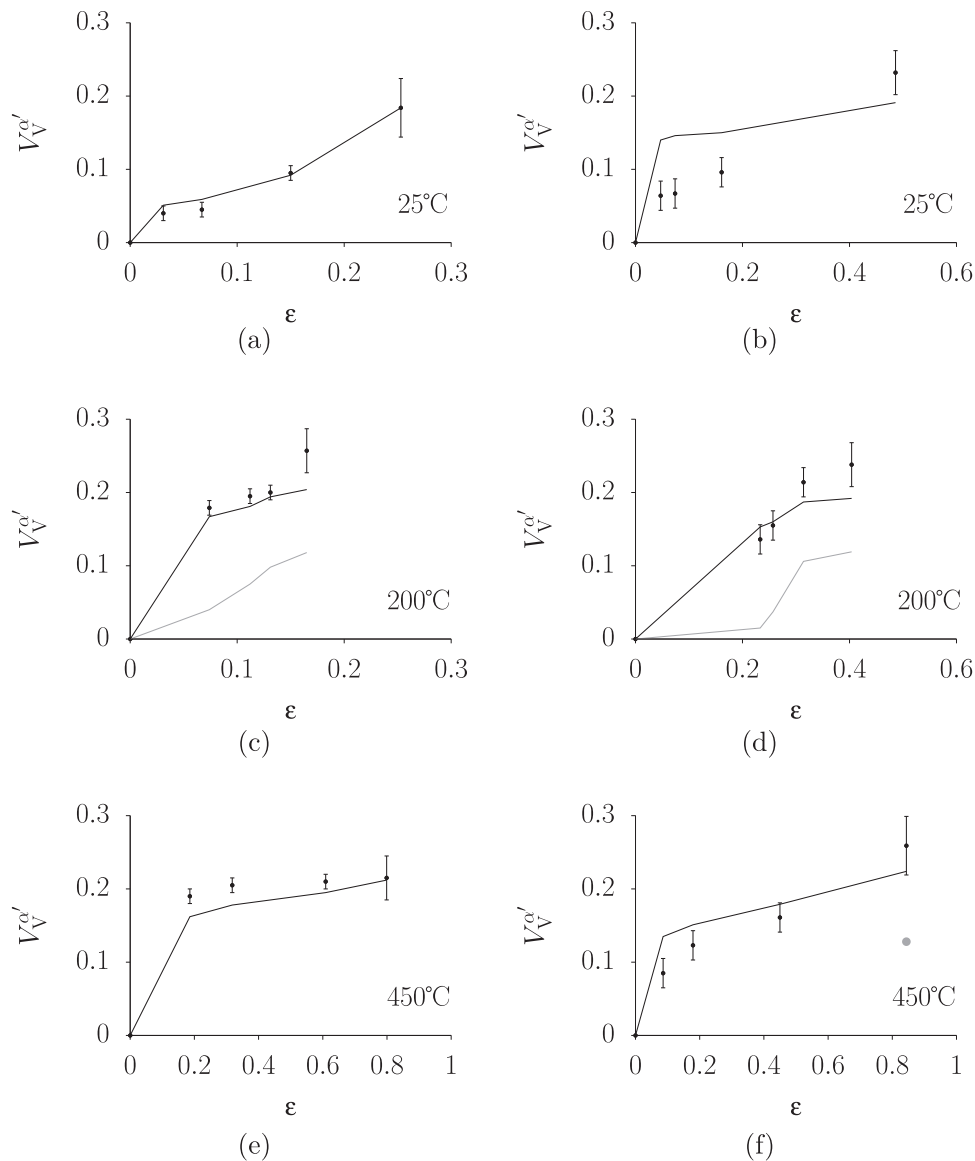


Fig. 10. Calculated volume fraction of martensite. (a, c, e) Alloy A and (b, d, f) Alloy B. In (c, d), the lighter curves represent the amount of martensite that forms at the test temperature and the darker curves include that which also forms during cooling from the test temperature. In (f) there is only one circumstance (light point) where martensite forms at the tensile test temperature, when the strain is greatest.

7. Mechanical stability of retained austenite

Martensite is triggered when the chemical free energy change $\Delta G^{\gamma\alpha'} = G^{\alpha'} - G^{\gamma}$ reaches a critical value accompanying the $\Delta G_{M_S}^{\gamma\alpha'}$, in the context of transformation without any composition change [e.g., 25]. The martensite-start temperatures were measured using dilatometry (Figs. 9a and b) to be 236 °C and 164 °C, for Alloys A and B respectively. On combining these measurements with free energy calculations, the critical values of $\Delta G_{M_S}^{\gamma\alpha'}$ are found to be -2511 and -800 J mol^{-1} for Alloys A and B respectively; these will be of use later when analysing the combined effects of undercooling and stress on the evolution of martensite. The simplest way to achieve this given the M_S temperature is to use the Koistinen and Marburger equation [26]:

$$V_V^{\alpha'} = V_T^{\gamma} (1 - \exp\{\beta[M_S - T_Q]\}) \quad (1)$$

where $V_V^{\alpha'}$ is the volume fraction of martensite, V_T^{γ} is the volume fraction of retained austenite prior to cooling to a temperature $T_Q \leq M_S$. The coefficient β is empirical and was obtained approximately by fitting the equation to experimental dilatometric-data as shown in Figs. 9c and d.

We now have all the tools in place to estimate the stimulation of

martensite by applied stress, which would in the present case increase the martensite-start temperature via the contribution of an additional term $U \approx -0.86 \times \sigma$ to the free energy of transformation, where the stress is expressed in MPa [28,29]. However, the coefficient 0.86 is for the case where the stress induces the formation of martensite plates that are optimally oriented with respect to the tensile axis. This cannot happen in practice for polycrystalline austenite because the transformation crystallography determines the plate orientation which can only approximately match the optimal orientation. The actual coefficient is expected therefore to be less than 0.86, and was established by fitting to be ≈ 0.75 , a value used in subsequent calculations. The net driving force for transformation that accounts for stress at the temperature at which the tensile test is conducted, is therefore given by:

$$\Delta G_{\sigma}^{\gamma\alpha'} = \Delta G_T^{\gamma\alpha'} + U \quad (2)$$

with martensite being triggered when this reaches the critical value $\Delta G_{M_S}^{\gamma\alpha'}$ – this stress-affected M_S temperature can then be used with Eq. (1) to calculate the volume fraction of induced martensite.

The results of these calculations are listed in Tables 5. Fig. 10 illustrates the data, with the curves representing calculated values. In

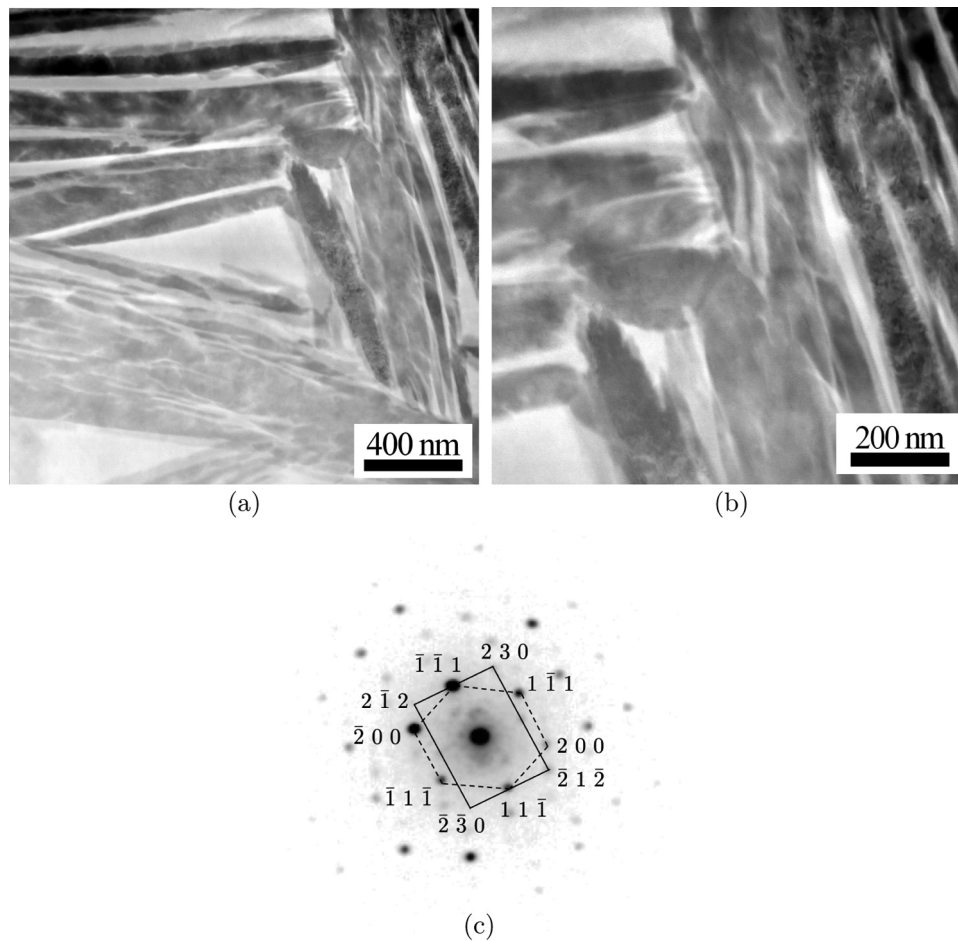


Fig. 11. STEM dark-field image of Alloy A as transformed. (a) Showing the film and blocky austenite following testing at 200 °C. (b) dark field high resolution STEM image. It should be noticed that testing at 200 °C causing particles of cementite to form within the austenite films. (c) Corresponding diffraction pattern.

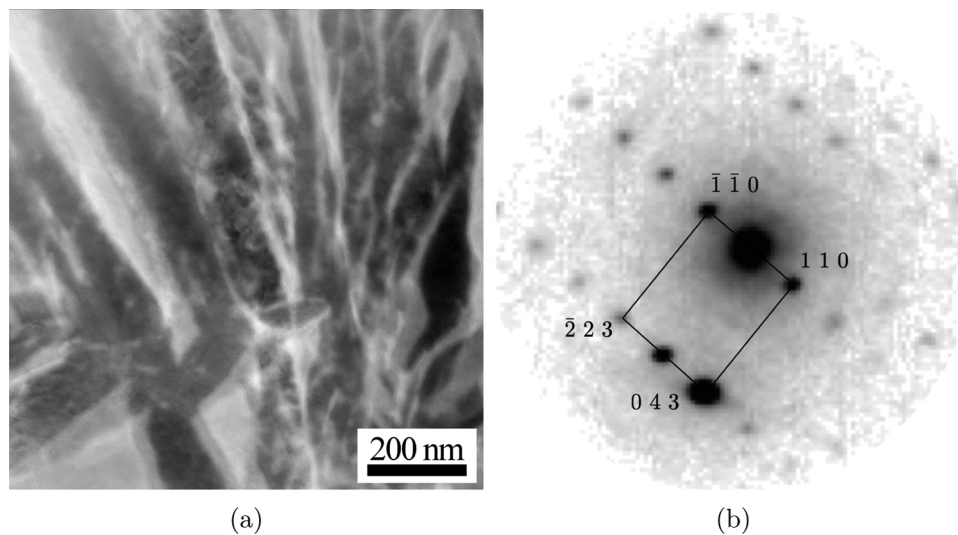


Fig. 12. STEM dark-field image of Alloy A as transformed. (a) Showing the film and blocky austenite following testing at 4500 °C. (b) Corresponding diffraction pattern of cementite particles.

some cases, the amount of martensite that forms at the test temperature is supplemented by that which forms during cooling from that temperature. Note that the strains plotted represent local strains measured on the cross-section of the tensile specimen at that location, where the retained austenite content was also determined. The necked regions therefore are identified with greater strains than recorded over the

gauge length of the tensile test specimen.

8. Conclusions

The steels studied here were designed originally for thermal stability, i.e., any austenite retained following partial transformation to

bainitic ferrite should be maintained at reasonably high temperature. Whereas there are many studies on the deformation-induced transformation of austenite into martensite, the alloys studied here have revealed some unusual behaviour, partly because of their rich chemical compositions but also because tensile tests were conducted at a variety of temperatures.

- Testing at ambient temperature resulted in tensile curves that are typical of very strong materials. There was, however, limited ductility, given the strength levels observed which are well in excess of 1.5 GPa.
- Surprisingly, tensile testing at 200 °C led not only to an increase in strength but at the same time, a remarkable increase in ductility for both alloys.

When the temperature is raised, the thermodynamic stability of the austenite increases, which should make it more difficult to obtain martensite. Previous work on δ – TRIP steel [24], which is designed for low-strength applications (about 70% allotriomorphic ferrite, 15% bainitic ferrite and the residue retained austenite) has demonstrated that the ductility decreases by testing at 100 °C because the austenite then does not transform, in which case the work hardening capacity due to the TRIP effect is lost. The present work demonstrates the opposite tendency, albeit for completely different steels, that an increase in the test temperature has led to an increase in strength and an increase in ductility, especially, uniform ductility. The explanation for the present observation is that although the thermodynamic stability of the austenite in the microstructure has definitely been increased at 200 °C, it still transforms into martensite during deformation. However, the marginal stability allows it to transform in a more gradual manner so that plastic instability is delayed, leading to the simultaneous increase in strength and ductility. It is well known [11], that the austenite must have an optimum stability to martensitic transformation if necking is to be delayed. It seems that at room temperature, in both the alloys studied, it transforms too rapidly.

- When testing the structure at 450 °C, there is a dramatic collapse in the uniform ductility due to the rapid onset of plastic instability. This is because the austenite no longer is able to transform into martensite during the course of the testing at 450 °C. In Alloy B, an additional austenite formed at 450 °C, as proven by dilatometric and hardness data. The austenite then becomes unstable to transformation during cooling to ambient temperature, leading to hardening in the deformed region. It is important to note that this hardening is not due to transformation during deformation. The results are quite exciting because the alloy systems studied have been proven to be ideal for examining the tensile behaviour as a function of the stability of the austenite.

The results presented here may be the first demonstration that if the austenite is unable to transform at all as in Alloy B then there is a dramatic drop in the ductility and strength of the material of the microstructure which is a mixture of bainitic ferrite and austenite.

Appendix A. Supplementary data

Supplementary data associated with this article can be found in the online version at [doi:10.1016/j.msea.2018.12.124](https://doi.org/10.1016/j.msea.2018.12.124).

References

- [1] H.K.D.H. Bhadeshia, Atomic mechanism of the bainite transformation, *J. Heat. Treat. Mater.* 72 (6) (2017) 340–345, <https://doi.org/10.3139/105.110338> <<https://doi.org/10.3139/105.110338>>.
- [2] J. Deliry, Nouveau carbure de fer transformation bainitique dans les aciers au carbone silicium, *Mem. Sci. Rev. Metall.* 62 (1965) 527–550.
- [3] J. Pomey, Revenu de la martensite et reaction bainitique inferieure: cas des aciers au carbone-silicium et des aciers au carbone, *Mem. Sci. Rev. Metall.* 63 (1966) 507–532.
- [4] E. Kozeschnik, H.K.D.H. Bhadeshia, Influence of silicon on cementite precipitation in steels, *Mater. Sci. Technol.* 24 (2008) 343–347.
- [5] H.K.D.H. Bhadeshia, D.V. Edmonds, Bainite in silicon steels: a new composition-property approach II, *Metal. Sci.* 17 (1983) 420–425.
- [6] H.K.D.H. Bhadeshia, D.V. Edmonds, Bainite in silicon steels: a new composition-property approach I, *Metal. Sci.* 17 (1983) 411–419.
- [7] F.B. Pickering, Mechanism of bainite formation in low-alloy steels containing up to 0.4% carbon, in: *Proceedings of the 4th International Conference on Electron Microscopy*, pp. 626–637. Springer Verlag, Berlin, 1958.
- [8] L.C. Chang, H.K.D.H. Bhadeshia, Austenite films in bainitic microstructures, *Mater. Sci. Technol.* (1995) 874–881.
- [9] F.G. Caballero, H.K.D.H. Bhadeshia, Very strong bainite, *Curr. Opin. Solid State Mater. Sci.* 8 (2004) 251–257.
- [10] H.K.D.H. Bhadeshia, The first bulk nanostructured metal, *Sci. Technol. Adv. Mater.* 14 (2013) 14202.
- [11] H.K.D.H. Bhadeshia, *Bainite in steels: theory and Practice*, 3rd edition, Maney Publishing, Leeds, U.K., 2015.
- [12] M. Peet, H.K.D.H. Bhadeshia, Surface relief due to bainite transformation at 473 K, *Metall. Mater. Trans. A* 42 (2011) 3344–3348.
- [13] N. Tsuji, Y. Ito, Y. Saito, Y. Minamoto, Strength and ductility of ultrafine grained aluminium and iron produced by ARB and annealing, *Scr. Mater.* 47 (2002) 893–899.
- [14] H.S. Hasan, M.J. Peet, H.K.D.H. Bhadeshia, Severe tempering of bainite generated at low transformation temperatures, *Int. J. Mater. Res.* 103 (2012) 1319–1324.
- [15] M. Peet, S.S. Babu, M.K. Miller, H.K.D.H. Bhadeshia, Tempering of low-temperature bainite, *Metall. Mater. Trans. A* 48 (3410–3418) (2017).
- [16] M.A. Santajuana, R. Rementeria, M. Kuntz, J.A. Jimenez, F.G. Caballero, C. Garcia-Mateo, Low-temperature bainite: a thermal stability study, *Metall. Mater. Trans. A* 49 (6) (2018) 2026–2036.
- [17] C.N. Hulme-Smith, I. Lonardelli, M.J. Peet, A.C. Dippel, H.K.D.H. Bhadeshia, Enhanced thermal stability in nanostructured bainitic steel, *Scr. Mater.* 69 (2013) 191–194.
- [18] C.N. Hulme-Smith, H.K.D.H. Bhadeshia, Mechanical properties of thermally-stable, nanocrystalline bainitic steels, *Mater. Sci. Eng.: A* 700 (2017) 714–720, <https://doi.org/10.1016/j.msea.2017.04.110> (URL: <<http://linkinghub.elsevier.com/retrieve/pii/S0921509317305919>>).
- [19] C.N. Hulme-Smith, The thermal stability of bulk nanocrystalline steels, PhD thesis, University of Cambridge, 2016.
- [20] H.M. Rietveld, A profile refinement method for nuclear and magnetic structures, *J. Appl. Crystallogr.* 2 (1969) 65–71.
- [21] B.H. Toby, R factors in Rietveld analysis: how good is good enough? *Powder Diff.* 21 (01) (2006) 67–70, <https://doi.org/10.1154/1.2179804> <<http://journals.cambridge.org/abstract/S0885715600003250>>.
- [22] D.J. Dyson, B. Holmes, Effect of alloying additions on the lattice parameter austenite, *J. Iron Steel Inst.* 208 (1970) 469–474.
- [23] C. Garcia-Mateo, F.G. Caballero, T. Sourmail, M. Kuntz, J. Cornide, V. Smanio, R. Elvira, Tensile behaviour of a nanocrystalline bainitic steel containing 3 wt% silicon, *Mater. Sci. Eng.: A* 549 (2012) 185–192, <https://doi.org/10.1016/j.msea.2012.04.031> <<http://www.sciencedirect.com/science/article/pii/S0921509312005527>>.
- [24] S. Chatterjee, M. Muruganath, H.K.D.H. Bhadeshia, δ -{TRIP} Steel, *Mater. Sci. Technol.* 23 (07) (2007) 819–827.
- [25] L. Kaufman, M. Cohen, Thermodynamics and kinetics of martensitic transformation, *Progress. Metal. Phys.* 7 (1958) 165–246.
- [26] D.P. Koistinen, R.E. Marburger, A general equation prescribing the extent of the austenite-martensite transformation in pure iron-carbon alloys and plain carbon steels, *Acta Metall.* 7 (1959) 59–60.
- [27] H.-S. Yang, H.K.D.H. Bhadeshia, Uncertainties in the dilatometric determination of the martensite-start temperature, *Mater. Sci. Technol.* 23 (2007) 556–560.
- [28] J.R. Patel, M. Cohen, Criterion for the action of applied stress in the martensitic transformation, *Acta Metall.* 1 (05) (1953) 531–538.
- [29] S. Denis, E. Gautier, A. Simon, G. Beck, Stress-phase-transformation interactions - basic principles, modelling and calculation of internal stresses, *Mater. Sci. Technol.* 1 (1985) 805–814.